Chemical Physics 434 (2014) 1–10

Contents lists available at ScienceDirect

Chemical Physics

journal homepage: www.elsevier.com/locate/chemphys

Structural, optical and photocatalytic properties of TiO_2/SnO_2 and SnO_2/TiO_2 core–shell nanocomposites: An experimental and DFT investigation

Pawan Chetri *, Priyanka Basyach, Amarjyoti Choudhury

Dept. of Physics, Tezpur University, Napaam, 784028 Tezpur, India

ARTICLE INFO

Article history:
Received 26 November 2013
In final form 12 February 2014
Available online 22 February 2014

Keywords:
Core–shell
XRD
TEM
BET
DFT
Photocatalytic

ABSTRACT

We employed an efficient and cost effective method to synthesize core–shell TiO_2/SnO_2 and inverted core–shell SnO_2/TiO_2 nanocomposites and investigated their visible light photo catalytic activity for degradation of dye methyl orange. We carried out techniques such as XRD and TEM for the structural verification while UV–Visible and photoluminescence spectra for the optical characterization. BET is done to reveal pore diameter and surface area of prepared nanosystems. We have also performed DFT based calculation using VASP 5.2 to calculate density of states. The analyses of density of states indicate a higher photocatalytic efficiency of core–shell TiO_2/SnO_2 nanostructures and which we indeed observe through experiment as well.

1. Introduction

Semiconductor nanostructures currently grabbed the eyes of researchers as potential candidate for application in photocatalysis, photovoltaic devices. Recently, applications to environmental cleanup have emerged as important areas in heterogeneous photocatalyis [1]. Even though various works have been reported on the photocatalytic activity of other semiconductors such as SnO_2 [2], ZnO [3], Nb_2O_5 [4], CeO_2 [5], $SrTiO_3$ [6], CdS, HgS, ZnS, CdSe, Ga_2S_3 [7] and CdTe [8]. The prevalence of work has been focused on TiO_2 because of its appropriate thermodynamical positions of valence and conduction band edges for redox reactions, long term stability, low cost, non toxicity, resistance to photo and chemical corrosion [9,10]. Although TiO_2 has been considered as an ideal material for photocatalysis purpose but possesses certain restrictions such as poor absorbance in the visible regime and rapid recombination of photogenerated electron/hole pairs. These limitations are lessened by doping, coupling or coating the material with other promising semiconductor materials [11]. Coating a lower band gap nanomaterial by a higher band gap material yields core–shell nanostructures where the cores and shells may be any kind of colloidal particles, i.e. metals, insulators and all classes of semiconductors [12]. Also, it has been reported about inverted core–shell nanostructures where the core material is typically a higher band gap material and the shell material is a lower band gap material [13]. Recent works are progressing on core–shell Ag_2S/HgS nanostructures in which varying the shell thickness, a transition from TYPE 1 (both electron and hole wave functions are distributed over the entire nanocrystal) to TYPE 2 (electron and hole are spatially separated between the shell and core) is observed [12].

Transition metal oxides are found to exhibit significance impact in photocatalysis and they show special properties such as enhanced photoluminescence and chemical reactivity. Also they seem to show enhanced photocatalytic behavior due to large surface area. Currently the typical composite nanostructures like core–shell nanostructure are fabricated for the inside nanorods with outside covered layers e.g. TiO_2/ZnO, ZnO/MgO and ZnO/Er_2O_3 [14]. Jung and his co workers reported on photocatalytic activity of core–shell TiO_2/MgO nanostructures where $Mg(OH)_2$ gel was topoactically decomposed on TiO_2 particle surface resulting in highly nanoporous MgO coated TiO_2 particles. The highly hygroscopic and nanoporous MgO shell was used to absorb more water molecules and hydroxyl groups from the environment to achieve an enhanced photocatalytic property of the core–shell particles as compared to the uncoated TiO_2 counterpart [15]. In a recent report, TiO_2/C core–shell composite nanoparticles were fabricated in a specially made Swageok cell by a simple and efficient single step method at different temperatures. The as synthesized samples were tested

* Corresponding author. Tel.: +91 3712267120; fax: +91 3712267005.
E-mail address: pawan11@tezu.ernet.in (P. Chetri).

http://dx.doi.org/10.1016/j.chemphys.2014.02.007
0301-0104/

for photochemical activity for 4-chlorophenol degradation. The photobleaching studies of methylene blue were also executed under sunlight. It was found that the TiO_2/C samples showed higher photocatalytic activity than TiO_2 nanoparticles [16]. Akurati and his co workers reported on one step flame synthesis of SnO_2/TiO_2 composite nanostructures for photocatalytic applications [17]. Also, SnO_2 nanoparticles embedded on TiO_2 nanofibers were fabricated by a simple electrospinning method possessing highly efficient photocatalytic activity for Rhodamine B dye under UV light [18].

Recently, good quality works are progressing on core–shell nanocomposites using first principle calculation. Authors [19–21] have explained photocatalytic phenomena using DFT. Li et al. [20] and Tang et al. [21] established relation between experimental and theoretical investigation. In our work we have successfully synthesized TiO_2/SnO_2 (TS) and SnO_2/TiO_2 (ST) core–shell nanocomposites and compared properties of each core–shell to bare SnO_2 and TiO_2 nanoparticles. Also a DFT based calculation was carried out as a support to the experimental results where we prepared a model of SnO_2/TiO_2 and TiO_2/SnO_2 and the structures are optimized to the minimum energy configuration. The conclusion drawn from the partial densities of states are attempted to correlate with the visible light photocatalytic degradation of methyl orange (MO).

2. Experimental section

For the synthesis of TiO_2 nanoparticles, we followed a standard procedure where titanium isopropoxide, $Ti\{OCH(CH_3)_2\}_4$, was mixed with 2-propanol in 2:5 ratio and stirred for 30 min for homogenous mixing. Then a few drops of water were added to initiate the reaction while SnO_2 nanoparticles are prepared following [22] only with an increment of pH to 11. To the prepared TiO_2 nanoparticles, SnO_2 solution was added dropwise which was synthesized by the above method. Then it was allowed to stir for 4–5 h followed by centrifuging then drying to obtain core–shell TiO_2/SnO_2 nanostructures. To the SnO_2 nanoparticles, TiO_2 solution (mixture of titanium iso propoxide and few drops of water) is added dropwise and stirred for 2–3 h followed by centrifuging and drying to get the inverted core–shell SnO_2/TiO_2 nanocomposites.

Crystal structures of the nanoparticles are studied with Rigaku Miniflex X-ray diffractometer equipped with intense CuKα radiation (λ = 1.54 Å), at a scanning rate of 1°/min and in the scanning range from 10° to 70°. High resolution transmission electron microscope (HRTEM) images of the prepared nanoparticles are obtained with JEOL JEM 2010 transmission electron microscope operating at a voltage of 200 kV. UV–Vis absorption spectra of all SnO_2 nanoparticles are taken in diffuse reflectance mode (DRS) in Shimadzu 2450 UV Vis spectrophotometer. Photoluminescence (PL) spectra are monitored in a Perkin Elmer LS spectrometer. Nitrogen adsorption–desorption isotherms were measured at 77 K in a Quantachrome iQ autosorb analyzer. Surface area was determined using multipoint Brunauer–Emmett–Teller (BET) method. The pore size distributions of the prepared samples were determined based on Barett–Joyner–Halenda (BJH) model [23].

Photocatalytic activity of all the prepared samples are studied by monitoring the decrease of the maximum absorbance of methyl orange (MO) at 464 nm. The intensity of visible light used for irradiation is 2.3 mW/cm^2. For carrying out the degradation experiment, 50 mg of each of the prepared nanoparticles was added to 50 mL of methyl orange solution (with an initial methyl orange concentration of 10 mg L^{-1} dissolved in distilled water) taken in four separate 100 mL beaker, with an initial methyl orange concentration of 10 mg L^{-1}. The MO solution loaded with each catalyst was stirred in dark for 45 min for adsorption–desorption equilibrium and for pre concentration of the dye solution on the semiconductor surface. The catalyst loaded dye solution was placed in a UV–vis chamber at a distance of 6 cm from UV/Vis light. The irradiation time interval was chosen to be 10, 20, 40 and 60 min respectively. After complete irradiation, each solution was centrifuged at 10,000 rpm to get the catalyst free irradiated MO solution. 5 ml of each of the irradiated MO solution was taken for absorption measurement. The percent degradation of MO solution is given by

$$\%D = \left(\frac{A_0 - A_t}{A_0}\right) \times 100$$

where A_0 is the absorbance of unirradiated, without catalyst loaded methyl orange solution and A_t is the absorbance of catalyst degraded MO solution, irradiated for 10, 20, 40 and 60 min respectively. To investigate whether MO undergoes self degradation, the methyl orange solution is irradiated under visible light for the aforementioned time and there was no self degradation of MO.

For kinetic analysis the following equation is adopted

$$-\ln(A_0/A_t) = kt$$

where k is rate constant of the reaction. The slope of the linear fit of the plot of $\ln(A_o/A_t)$ vs. irradiation time (t) (as shown in Fig. 11) gives the value of rate constant.

We performed density functional calculations using generalized gradient approximation (GGA) functional with Perdew–Burke–Ernzerhof (PBE) to describe the electron–electron exchange and correlation effects. To describe the electronic structures more accurately, the GGA + U method was adopted with the strong on-site coulomb repulsion among the localized Ti3d electrons. The effective Hubbard parameter $U_{eff} = U–J$, which accounts for the on-site coulomb repulsion for each affected orbital. U_{eff} = 8.47 eV is considered for the calculation of density of states [24]. We have used U_{eff} = 0 eV for Sn4d electrons as it has no contribution near the Fermi level. The density functional theory (DFT) equations are solved via projector augmented wave (PAW) method using plane wave basis set as implemented in Vienna Ab Initio Simulation Package (VASP) and interfaced with MedeA technology platform. The minimum energy state is computed by varying the internal position of atoms until the residual force is 0.01 eV/Å. A 7 × 5 × 1 K-mesh is used in Brillouin Zone with origin shifted to gamma point. Methfessel–Paxton type of smearing is used with smearing width of 0.2 eV.

3. Results and discussions

3.1. Structural characterization

The diffraction peak of the samples (shown in Fig. 1) corresponds to rutile phase of SnO_2 (JCPDS 41-1445) and anatase phase

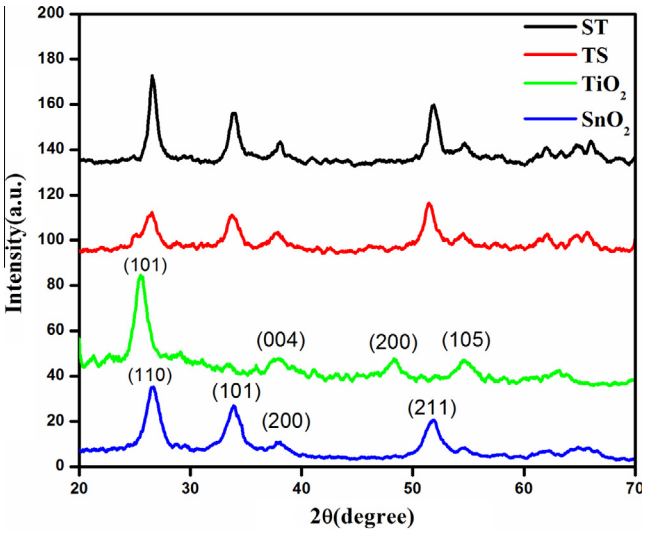

Fig. 1. X-ray diffraction of ST, TS, TiO_2 and SnO_2.